Proceedings of the 25th International Conference on
Port and Ocean Engineering under Arctic Conditions
June 9-13, 2019, Delft, The Netherlands

Investigation of mixed mode fracture of L-shaped sea ice beams

Igor I. Gribanov[1], Aleksey V. Marchenko[2], Andrii Murdza[3], Rocky S. Taylor[1], Robert Sarracino[1]
[1] Memorial University of Newfoundland, St.John's, Canada
[2] The University Centre in Svalbard, Longyearbyen, Svalbard and Jan Mayen
[3] Thayer School of Engineering, Dartmouth College, Hanover, USA

ABSTRACT

Modeling the fracture behavior of ice during mixed-mode loading is difficult. Historically, fracture testing in the field has focused primarily on experimental conditions such as flexural or tensile loading, which results in failure dominated by a single mode. Between 2014 and 2016, nine field experiments were performed on L-shaped cantilever beams where the deformation was a combination of bending and torsion. Two distinct fracture modes were recorded. In four of the nine cases, the failure occurred at the free end of the beam due to bending, and in five remaining cases, the failure occurred at the root of the beam due to torsion. Fracture paths are difficult to model under such conditions since they are influenced not only by geometry and loading conditions but also are affected by the variability of the material, including natural flaws present in the ice. In the current study, a cohesive zone model is applied to simulate the dynamic fracture processes in L-shaped beams. Evolution of the stress distribution on the surface of the beam is modeled for the duration of the loading process, showing how it changes with progressive accumulation of damage in the material, as well as the development of cracks. An analytical model is proposed for estimating the breaking force based on the dimensions of the beam, flexural and tensile strengths of the material. Dimensionless constants in the model are determined as the best fit for the simulation results. Finally, the experimental data obtained from the 2014-2016 tests are re-evaluated to infer the flexural and tensile strength of ice based on the proposed analytical model.

KEY WORDS: Ice fracture, Ice mechanical tests, Cohesive zone model, Finite element analysis

INTRODUCTION

Experimental measurements of mechanical properties of ice are performed quite regularly. Standardized testing methods are described by Schwarz et al. (1980), and, more recently, by International Towing Tank Conference (ITTC) Recommended Procedures for testing ice properties. While there are several techniques for measuring flexural and compressive strengths, the only recommended method for measuring shear strength is the punch through test in which a hole is punched in a sheet of ice. An alternative way of investigating the shear strength was

suggested by Murdza et al. (2016), whose method is similar to in-situ plain beam loading, but instead uses an L-shaped cantilever beam. In such test, a pure bend is mixed with a torsional load, resulting in a "complex bend" – a superposition of bending (tensile) and plane (shear) stresses. Such loads are common in natural motion and breakup of ice, where the failure criterion cannot be formulated in terms of flexural strength alone.

Nine experiments on L-shaped cantilever beams were conducted between November 2014 and March 2016. The following information was recorded for each test:

- dimensions of the beam
- loading direction: upward or downward
- type of ice: sea or freshwater
- temperature and average salinity of ice
- force-time and displacement-time curves
- maximal indentation force and the corresponding indenter displacement
- angle and shape of the crack

Additionally, finite element analysis was performed to estimate the distribution of stress on the surface of the beam. For the constitutive model of ice, isotropic linear elastic material was selected. By inspecting the first and third principal stresses areas of stress concentrations were located. However, those areas did not coincide with the experimentally observed fracture paths.

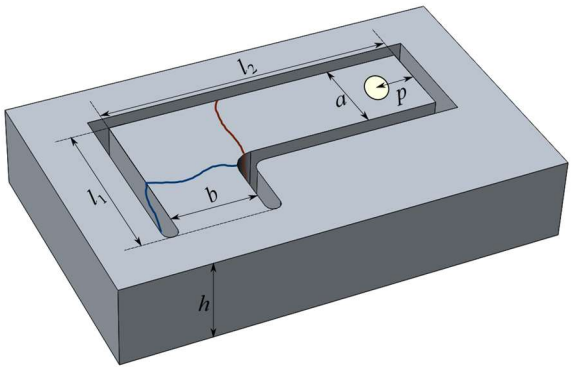

Figure 1. Dimensions of the L-shaped beam, indenter application point and two crack paths, which correspond to the free end fracture (shown in red color) and the fixed end fracture (shown in blue).

While none of the fracture paths were the same in the experiment, their locations can be classified into two groups: (1) at the free end and (2) at the fixed end (Figure 1). The experiments and subsequent simulations showed that "in-between" option is unlikely, and fractures usually occur on either side of the bend. Failures at the free end are analogous to the experiments with plain cantilever beams, failing in pure flexure. In such a case, even if the shear stresses were present, the maximum recorded load corresponds to the sample strength in transverse bending. On the other hand, failures at the fixed end correspond to torsional failure, where shear strength plays the main role.

The present work attempts to re-evaluate the obtained experimental data with the aid of the recently implemented cohesive zone model for ice fracture (Gribanov et al., 2018) and calculate the corresponding flexural and tensile strengths. Additionally, the analytical solution is suggested to determine whether the sample will break by flexure or torsion. The analytical approach may be helpful for quick estimates of the breaking force and type of failure, which depends on the dimensions of the beam and mechanical properties of the material. For brevity, beam dimensions will be presented as ordered list of the form $\{l_1, l_2, a, b, h\}$ with values expressed in meters.

COHESIVE ZONE MODELING

The non-linear behavior of ice was summarized by Sanderson (1988). For the processes with large deformations and fragmentation, researchers still struggle to formulate a suitable constitutive model of ice. Various approaches to modeling ice fracture include continuum models for material damage (Kavanagh, 2018), wing crack growth (Kolari, 2017), analysis based on the specific energy of fracture (Tsuprik et al., 2017), probabilistic fracture mechanics (Taylor and Jordaan, 2015) and cohesive zone model (Gribanov et al., 2018). The latter was successfully applied to analyze uniaxial compressive and tensile tests of ice samples. The Park-Paulino-Roesler formulation (Park et al., 2009; Park and Paulino, 2013) has eight parameters that determine traction-separation curves of cohesive zones in normal and tangential directions. This flexibility allows to model damage accumulation and fracture in a wide range of materials including ice.

Establishing the parameters of a CZ model is a non-trivial task. Experimental measurements of ice strength usually provide a single quantity, such as the maximum indentation force before failure. This quantity can be converted to either flexural, tensile or shear strength, depending on the type of the experiment. On the other hand, the CZ model requires such values as specific fracture energies, normal and cohesive strengths σ_{max} and τ_{max}, shape coefficients of traction-separation curves and initial slopes of these curves. Some of the required values can be established based on small-scale laboratory tests, but the main difficulty lies in determining the normal and tangential strengths of cohesive zones σ_{max} and τ_{max} based on the limited number of experimental results.

The first simulation is performed on a beam with dimensions $\{1.05,1.95,0.55,0.55,0.56\}$. A tetrahedral mesh is created with *gmsh* library, with the element count of 8582 and cohesive zone count of 8339. In this and subsequent tests, the radius of rounding on the inner side of the beam is set to 0.2m (twice the size of the gap). Cohesive zones are inserted between the elements in the area where the fracture is expected (Figure 2). Parameters of the material and cohesive zones are listed in Table 1. An attempt is made to use simulation parameters that result in breaking forces similar to the ones observed in the field experiments. The goal for performing the simulation is to observe the evolution of stress distribution and to generate a set of data points for differing beam dimensions, keeping the material parameters fixed.

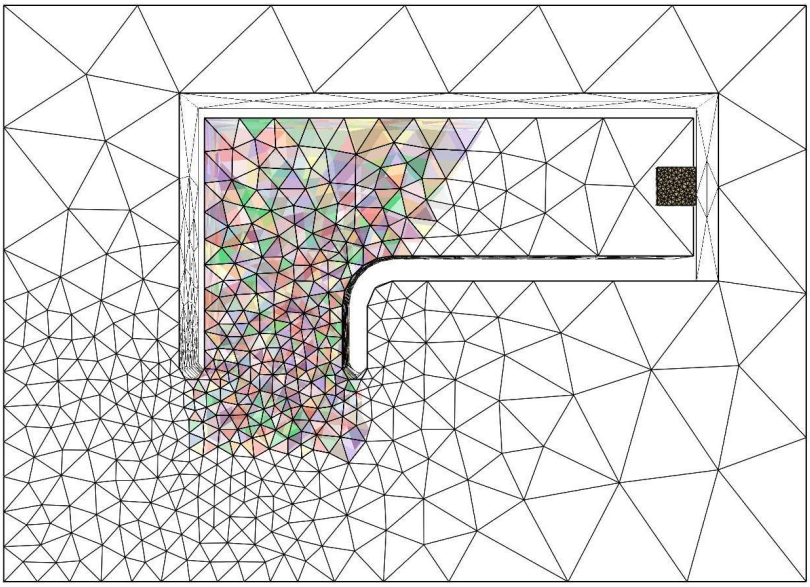

Figure 2. Tetrahedral mesh for FE simulation. Cohesive zones are inserted between the highlighted elements. Indenter measuring 15x15 cm applies force to the free end of the beam.

Table 1. Parameters of cohesive zones and elastic elements.

Notation	Description	Value
σ_{max}	Normal cohesive strength	120 kPa
τ_{max}	Tangential cohesive strength	140 kPa
ϕ_n, ϕ_t	Mode I and II fracture energies	3 J m^{-2}
α, β	Shape of traction-separation curves (determine brittleness)	4
λ_n, λ_t	Non-dimensional slope indicators in PPR model	0.015
E	Young's modulus	5 MPa
υ	Poisson's ratio	0.3
ρ	Density of the material	916.2 kg/m^3

The force is applied at the free end of the beam via rectangular indenter moving downwards at 1.7 mm/s (Figure 3a). The graph of force on the indenter versus time is shown in Figure 3b. The initial time step is set to 0.1 s, and the adaptive algorithm decreases it to 0.1/2048 when needed. For brittle cylinders under torsional load the fracture usually has a helicoidal shape (Davis et al., 1982); in the current simulation, the fracture surface is slightly curved (Figure 3a). The fracture surface in the simulation compares favorably with fracture surfaces observed in the field experiments. In one of the field tests the root part of the beam, which remained attached to the ice cover after the beam failure, was cut off with a hand saw and placed on the wooden pallet in the way that the cut surface was on the bottom, in contact with the pallet, and the fracture surface was on the top (Figure 3c). The fracture surface is curved and inclined; the distance from the beam root to the fracture surface is smaller on the bottom of the beam; the distance from the beam root to the fracture surface on the bottom of the beam is smaller from the side of a shorter lever or at the rounding B in Figure 4a in Murdza et al. (2016). Thus, the fact that the fracture surfaces obtained in both simulation and field experiment are almost identical is a good sign of the accuracy of the simulation.

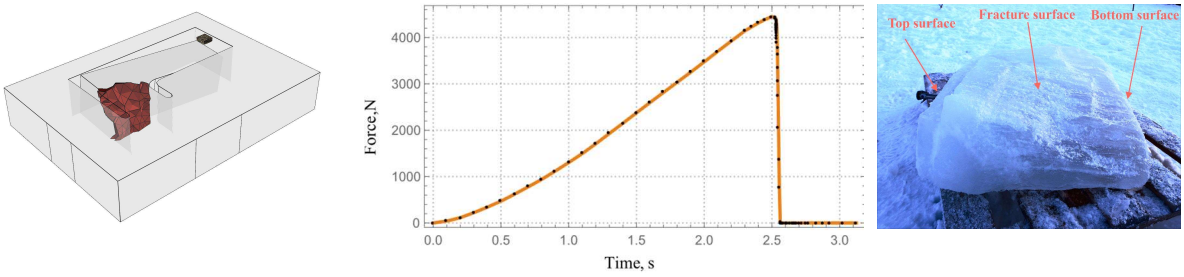

(a) (b) (c)

Figure 3. (a) Resulting fracture surface. (b) Force on the indenter vs. time. (c) A typical fracture surface obtained in the field test.

Evolution of the distribution of first principal stress is shown in Figure 4. At the initial stages of loading, two areas of high stress concentration develop (Figure 4a), where the values reach 66 kPa. Such stress concentration is not sufficient to damage cohesive zones, whose strength is about twice higher. In the initial stage, the distribution of stress on the surface is similar to the linear elastic case.

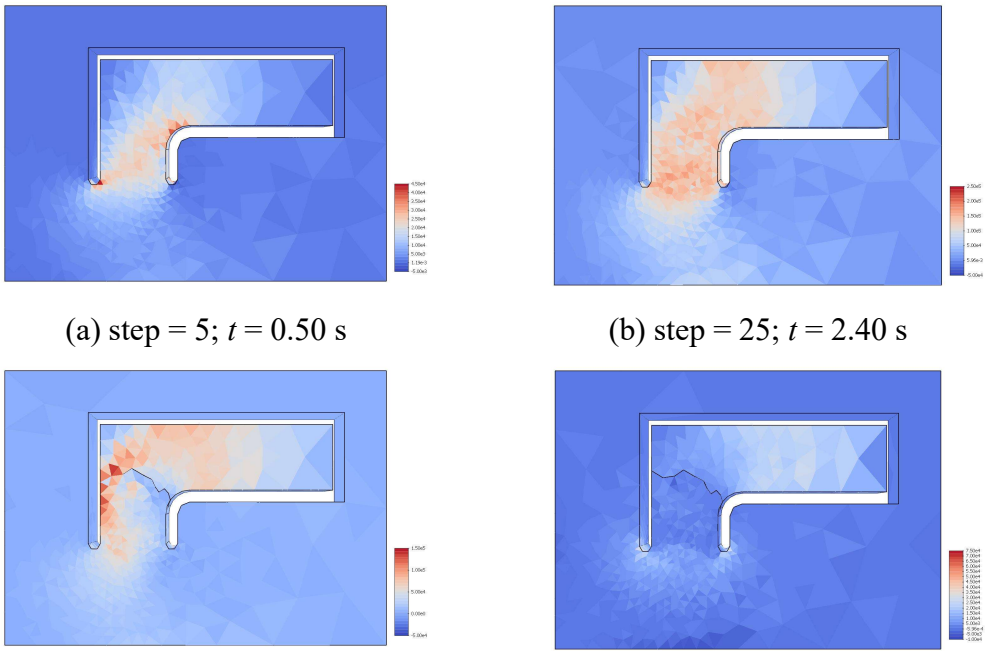

(a) step = 5; t = 0.50 s (b) step = 25; t = 2.40 s

(c) step = 44; t = 2.53 s (d) step = 57; t = 2.54 s

Figure 4. Distribution of the first principal stress over the top surface of the beam at various time steps. The units on the legends are Pascals.

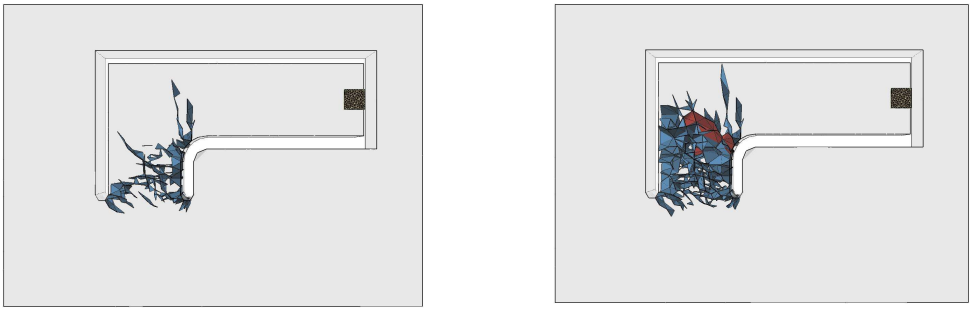

(a) step = 25; t = 2.40 s (b) step = 44; t = 2.53 s

Figure 5. Accumulation of damaged cohesive zones, shown in blue color, and propagating crack, shown in red.

First damaged cohesive zones appear on step 16 in the lower-left corner of the beam. At step 25 about 3% of cohesive zones become damaged (Figure 5a), and stress distribution is visibly different from the linear case (Figure 4b). Between steps 18 and 30, the maximum value of the first principal stress stays around 200 kPa and starts to drop when the fracture is initiated at step 30; a reduction of stress concentration is then seen near the propagating crack (Figures 4c, 5b). After the propagation is complete, the internal damage results in residual internal stresses (Figure 4d).

ANALYTICAL APPROACH

If the failure occurs at the free end, the process can be viewed as plain cantilever beam bending. The breaking force, which is determined by the flexural strength, can be approximated via equation for the elastic beam:

$$F = \frac{\sigma_f w h^2}{6l}, \tag{1}$$

where σ_f is the flexural strength, l is the length, w is the width and h is the height of the beam. Expression (1) is derived for the fixed-end plain beam and is not expected to yield precise results for the L-shaped beam, where the fracture is not perpendicular to the main axis and torsional deformation leads to non-symmetric stress distribution with areas of high stress concentration. This effect is influenced by the width of the fixed-end fragment, which expression (1) does not include. To account for the approximate application of formula (1), a dimensionless coefficient k is introduced. The length l is taken to be $(l_2 - b - p)$, where l_2 is the length of the free end, b is the width of the fixed end, and p is the point of application of the indenter (Figure 1). Substituting the length l into expression (1) yields the approximation for the breaking force

$$F_p = \frac{k\sigma_f a h^2}{6(l_2 - b - p)}. \tag{2}$$

In this and subsequent calculations, the indenter application point p is 0.075 m. By fitting equation (2) to the results of finite element simulations, the value of the dimensionless coefficient was found to be $k = 0.831$. It shows that the breaking force of the L-shaped beam is about 83.1% of the breaking force of a corresponding plain cantilever beam.

A different approach is taken when the fracture takes place at the fixed end. In such a case, the loading process is a combination of torsion and bending, and both components influence the breaking force. The bending component can be approximated as

$$F = \alpha \frac{\sigma_b b h^2}{6l_1}, \tag{3}$$

where α is a dimensionless constant, σ_b is the bending (flexural) stress and l_1 is the length of the fixed end. To estimate the torsional component, the beam is viewed as a solid rectangular cross-section to which a twisting moment is applied. The free end of the beam acts as a lever that applies torque $T = F\ (l_2 - p)/\beta$, where β is another dimensionless constant. Maximum shear stress on the surface of rectangular solid under torsional load is expressed as (Roark et al., 2012):

$$\sigma_t = \frac{3T}{bh^2}\left[1 + 0.6095\frac{h}{b} + 0.8865\left(\frac{h}{b}\right)^2 - 1.8023\left(\frac{h}{b}\right)^3 + 0.9100\left(\frac{h}{b}\right)^4\right]. \tag{4}$$

Formula (4) is derived with the condition $b \geq h$, where b is the width and h is the height of the beam. For the cases where $b < h$, parameters b and h must be swapped.

Stress tensor at the surface of the fixed end is written in the form

$$\sigma = \begin{pmatrix} \sigma_b & \sigma_t \\ \sigma_t & 0 \end{pmatrix}, \tag{5}$$

whose principal values are equal to

$$\sigma_1 = \frac{\sigma_b}{2} + \sqrt{\left(\frac{\sigma_b}{2}\right)^2 + \sigma_t^2}, \qquad \sigma_2 = \frac{\sigma_b}{2} - \sqrt{\left(\frac{\sigma_b}{2}\right)^2 + \sigma_t^2}. \tag{6}$$

The failure criterion is formulated as

$$\sigma_1 = \sigma_{ten}, \tag{7}$$

where σ_{ten} is the tensile strength on the surface, which is equal to flexural strength when $\sigma_t = 0$. The first principal direction is specified by equation

$$y = \frac{\sigma_1 - \sigma_b}{\sigma_t} x, \tag{8}$$

where the axes x and y are directed along the levers l_1 and l_2. The failure surface is perpendicular to the first principal direction and starts from the beam root because of the stress concentration. If $\sigma_t = 0$ then the failure surface is parallel to y-axis and corresponds to the crack in the beam root in bending failure.

Substituting expressions (3) and (4) into (7) yields

$$F_l = \begin{cases} \dfrac{\alpha\, \sigma_{ten}\, bh^2}{3l_1\left(1 + \sqrt{1 + \left(\dfrac{2\alpha(l_2 - p)}{\beta\, l_1}\gamma\right)^2}\right)}, & b \geq h \\ \dfrac{\alpha\, \sigma_{ten}\, bh^2}{3l_1\left(1 + \sqrt{1 + \left(\dfrac{2\alpha(l_2 - p)h}{\beta\, l_1\, b}\tilde{\gamma}\right)^2}\right)}, & b < h \end{cases} \tag{9}$$

Where

$$\gamma = 1 + 0.6095\frac{h}{b} + 0.8865\left(\frac{h}{b}\right)^2 - 1.8023\left(\frac{h}{b}\right)^3 + 0.91\left(\frac{h}{b}\right)^4,$$

$$\tilde{\gamma} = 1 + 0.6095\frac{b}{h} + 0.8865\left(\frac{b}{h}\right)^2 - 1.8023\left(\frac{b}{h}\right)^3 + 0.91\left(\frac{b}{h}\right)^4.$$

Expressions (2) and (9) agree very well with the results of the finite element simulation. That is, for the material with known flexural strength σ_f and tensile strength σ_{ten}, the breaking force of the L-shaped beam can be predicted. Expression (2) predicts the breaking force F_p in the flexural mode, and expression (9) predicts the mixed-mode failure F_l. The weakest of the two forces determines the actual location of the crack.

Comparison of the Analytical Solution with FEM Parametric Tests

Computer simulations allow to test the strengths of beams of varying dimensions quickly. A set of parametric FEM studies was conducted and summarized in Table 2. Material parameters were the same for all tests (Table 1). Results of the parametric studies are used to establish parameters for the analytical expressions.

Table 2. Series of parametric tests.

Varying parameter	Parameter name	Parameter range, [m]	Beam dimensions $\{l_1, l_2, a, b, h\}$	Number of tests
l_1	Length of the fixed end	0.9–1.3	{–, 1.7, 0.55, 0.55, 0.56}	20
l_1	Length of the fixed end	0.9–1.8	{–, 1.6, 0.5, 0.55, 0.5}	20
l_2	Length of the free end	1.3–3.0	{1.05, –, 0.55, 0.55, 0.56}	20
a	Width of the free end	0.3–0.6	{1.05, 1.95, –, 0.55, 0.56}	20
b	Width of the fixed end	0.15–0.85	{1.05, 1.95, 0.55, –, 0.56}	33
h	Thickness	0.15–0.90	{1.05, 1.95, 0.55, 0.55, –}	30

To determine the coefficients α and β, the best fit is found for expression (9) based on parametric FEM studies (Table 2). Parametric tests are separated into two fracture modes with the first group containing fractures at the free end (Figure 6) and the second group containing fractures at the fixed end (Figure 3a). The latter group is used for fitting coefficients α and β in expression (9). The obtained values of the coefficients are $\alpha = 2.758$ and $\beta = 4.588$. By performing a uniaxial tension simulation, the tensile strength of the simulated material is determined to be $\sigma_{ten} = 138501$.

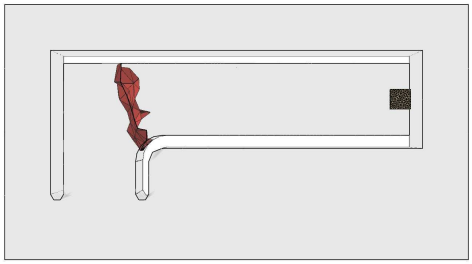

Figure 6. Simulated fracture at the free end of the beam.

The first parametric study varies the parameter l_1 for beams with dimensions {–, 1.7, 0.55, 0.55, 0.56} and {–, 1.6, 0.5, 0.55, 0.5}. Equation (9) accurately predicts the decrease of the breaking force with the increasing length l_1. Blue lines on Figure 7 correspond to the breaking force for flexural failure (at the free end), but the actual fracture takes place at the fixed end with lower force. Results of the finite element simulations show some variability due to the randomness in finite element meshing, but they follow the analytical prediction.

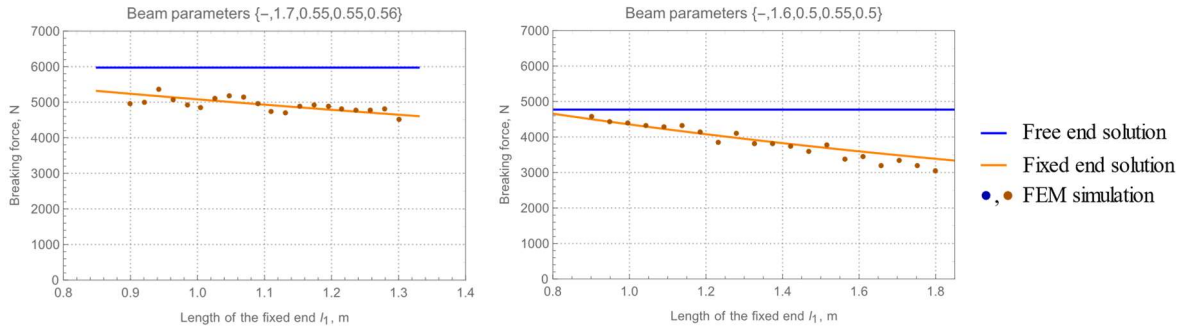

(a) (b)

Figure 7. Parametric study for varying length of the fixed end.

The next parametric study varies the length of the free end l_2 from 1.3 to 3.0 meters, with 20 gradations between (Figure 8a). The beam dimensions are {1.05, –, 0.55, 0.55, 0.56}. Up until the length of 2.19m, the beams break at the fixed end, whereas longer beams break at the free end. The point where the transition occurs is captured by the analytical model as the intersection of equations (2) and (9).

Parametric study of the width of the free end shows that wider beams result in higher breaking forces, but only in the region where the fracture occurs at the free end. After reaching a certain width, the wide free end becomes strong enough to sustain the load, and the fracture mode shifts to the fixed end, as illustrated in Figure 8b.

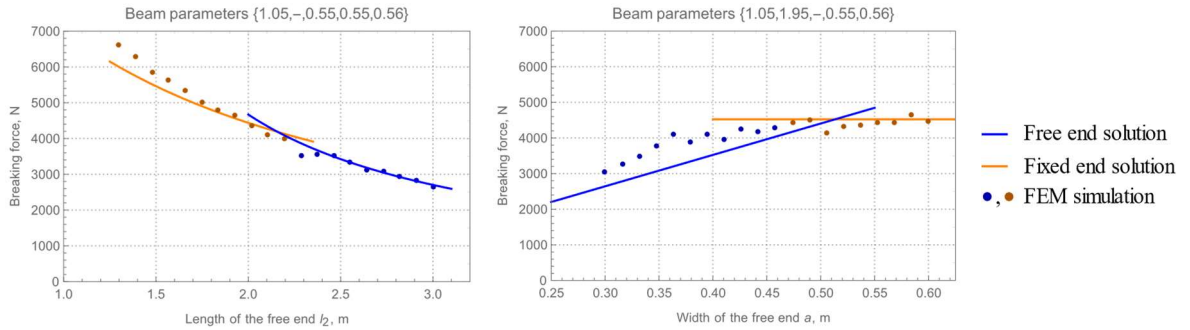

(a) (b)

Figure 8. Parametric study for varying (a) length of the free end, (b) width of the free end.

Two additional studies were conducted to verify the applicability of expression (9). Both studies expose the non-linear dependence between the breaking force and the beam dimensions. When the fixed end is narrow (Figure 9a) it fractures easily. However, the breaking force grows non-linearly with increasing width. After a certain width is reached, the fixed end becomes stronger than the free end and the fracture mode changes, which is reflected in Figure 9a. Varying the thickness of the sheet also has a non-linear relationship with the breaking force (Figure 9b). In both cases, the proposed analytical expressions (2) and (9) capture the complex relationship and give accurate predictions.

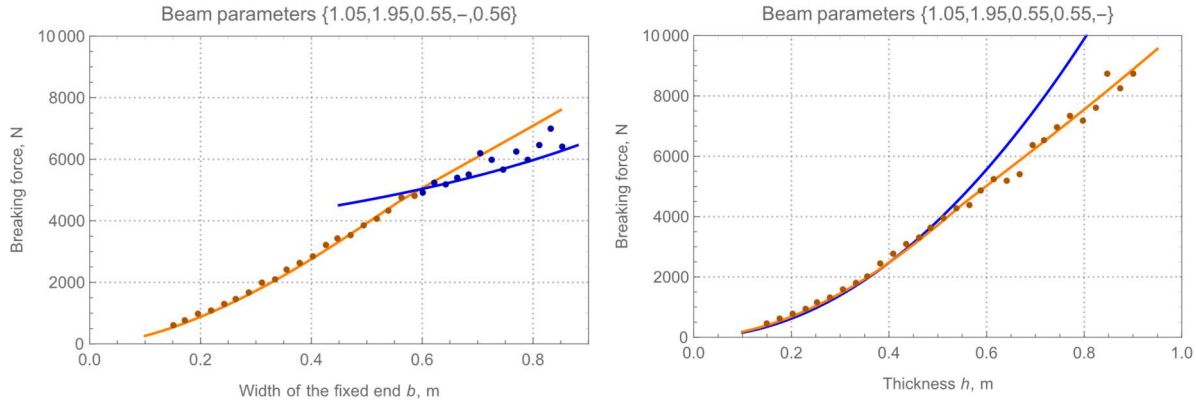

(a) (b)

Figure 9. Parametric tests for varying (a) width of the fixed end, (b) thickness of the sheet.

Application of the Analytical Model to the Field Test Data

The field tests performed by Murdza et al. (2016) recorded beam dimensions alongside with the breaking forces. By applying the proposed analytical model, additional information about the material can be inferred. When the fracture occurs at the free end, the flexural strength can be determined via equation (2). For the tests where fractures happened at the fixed end, tensile strength can be determined via equation (9). This data is calculated and summarized in Table 3.

Table 3. Calculated flexural/shear strength for experimentally obtained forces.

No.	Ice Type	l_1 [m]	l_2 [m]	a [m]	b [m]	h [m]	F_{max} [N]	σ_f [kPa]	σ_{ten} [kPa]
1	sea	1.05	1.95	0.55	0.55	0.56	6267	–	194
2	sea	1.2	2.1	0.6	0.6	0.53	3881	–	130
3	sea	1.2	2.08	0.6	0.65	0.6	4506	–	109
4	fresh	0.75	1.1	0.42	0.36	0.36	2559	–	173
5	fresh	0.68	1.15	0.4	0.44	0.36	3528	285	–
6	fresh	-	2.55	0.85	0.85	0.28	1436	231	–
7	sea	1.3	2	0.62	0.65	0.59	6897	269	–
8	sea	1.15	1.45	0.55	0.6	0.59	7064	189	–
9	sea	1.57	1.22	0.9	0.57	0.59	6142	–	147

DISCUSSION AND CONCLUSIONS

The tests presented in Table 3 were performed at three different locations. Even the samples 1-3 that come from the same site show high variability in tensile strengths, ranging between 109kPa and 194 kPa, which suggests that the tested ice contained random inclusions that influence test results. Marchenko and Sakharov (2017) performed laser scanning of the fractured surfaces and discovered the so-called "cheese ice," whose surface contained cylindrical holes. Therefore, non-homogeneous natural ice can differ in its mechanical properties even at the same test site.

Performing large-scale and medium-scale tests in the field is a labor-intensive task; and usually, only a small number of data points are collected. Computer simulations provide more insight about the fracture processes, allowing to run parametric studies. In the case of the L-shaped beam, it may be possible to predict, to some extent, whether the beam would break at the fixed or free end. This approach may be useful, for example, if the goal is to perform fixed-end torsional fractures only.

The proposed analytical approach has several simplifications. It does not account for the bending geometry of the beam and does not consider the progressive accumulation of damage. In comparison with the finite element modeling, however, the results are much faster to obtain, still providing good accuracy.

The finite element simulation accounts for the dynamics of the process, gradual accumulation of damage and redistribution of the stress during the loading process. The modeled loading curves, the locations of the cracks and their shapes generally agree with the experimental results. To some extent, simulation results depend on the mesh topology, and the predicted breaking force may be slightly different for different mesh geometries. Another drawback of the simulation is that it requires significant time to compute, i.e. about 20 minutes per test. It is formulated in terms of normal and tangential strengths of cohesive zones, which are not measured directly. Analytical expressions are easier to use and may be applied to estimate the force and type of fracture quickly.

ACKNOWLEDGEMENTS

The authors gratefully acknowledge funding from Hibernia Management and Development Company, Ltd. (HMDC), Terra Nova Development (Suncor Energy Inc. - Operator), InnovateNL and the Natural Sciences and Engineering Research Council of Canada (NSERC) for this work. Use of facilities and other practical support provided by C-CORE is gratefully acknowledged.

REFERENCES

Davis, H.E., Troxell, G.E., Hauck, G.F.W., 1982. The testing of engineering materials, 4th ed. ed. McGraw-Hill, New York.

Gribanov, I., Taylor, R., Sarracino, R., 2018. Cohesive Zone Micromechanical Model for Compressive and Tensile Failure of Polycrystalline Ice. Engineering Fracture Mechanics.

Kavanagh, M.B., 2018. Time-dependent aspects of fracture in ice (Doctoral dissertation, Memorial University of Newfoundland).

Kolari, K., 2017. A complete three-dimensional continuum model of wing-crack growth in granular brittle solids. International Journal of Solids and Structures 115–116, 27–42. https://doi.org/10.1016/j.ijsolstr.2017.02.012

Marchenko, N., Sakharov, A., 2017. Laser scanning in mechanical ice tests, in: 24th International Conference on Port and Ocean Engineering under Arctic Conditions. Busan, Korea.

Murdza, A., Marchenko, A., Sakharov, A., Chistyakov, P., Karulin, E., Karulina, M., 2016. Test with L-shaped cantilever beam for complex shear and bending strength, in: Proceedings of the 23rd IAHR International Symposium on Ice.

Park, K., Paulino, G., 2013. Cohesive Zone Models: A Critical Review of Traction-Separation Relationships Across Fracture Surfaces. Applied Mechanics Reviews 64, 060802. https://doi.org/10.1115/1.4023110

Park, K., Paulino, G.H., Roesler, J.R., 2009. A unified potential-based cohesive model of mixed-mode fracture. Journal of the Mechanics and Physics of Solids 57, 891–908. https://doi.org/10.1016/j.jmps.2008.10.003

Roark, R.J., Young, W.C., Budynas, R.G., Sadegh, A.M., 2012. Roark's formulas for stress and strain, 8th ed. ed. McGraw-Hill, New York.

Sanderson, T.J.O., 1988. Ice mechanics: risks to offshore structures. Graham & Trotman, London, UK ; Boston.

Schwarz, J., Frederking, R., Gavrillo, V., Petrov, I.G., Hirayama, K.-I., Mellor, M., Tryde, P., Vaudrey, K.D., 1981. Standardized testing methods for measuring mechanical properties of ice. Cold Regions Science and Technology 4, 245–253. https://doi.org/10.1016/0165-232X(81)90007-0

Taylor, R.S., Jordaan, I.J., (2015). Probabilistic fracture mechanics analysis of spalling during edge indentation in ice. Engineering Fracture Mechanics 134 (2015) 242-266.

Tsuprik, V., Bekker, A., Pomnikov, E., Ivolgin, E., 2017. Experimental Researching of the Specific Energy Mechanical Fracture of Ice by Method of Uniaxial Compression of Samples, in: 24rd International Conference on Port and Ocean Engineering under Arctic Conditions. Busan, Korea.